

The Effect of “Rogue” Active Regions on the Solar Cycle

Melinda Nagy¹ · Alexandre Lemerle^{2,3} ·
François Labonville² · Kristóf Petrovay¹ ·
Paul Charbonneau²

© Springer ●●●

Abstract

The origin of cycle-to-cycle variations in solar activity is currently the focus of much interest. It has recently been pointed out that large individual active regions with atypical properties can have a significant impact on the long term behaviour of solar activity. We investigate this possibility in more detail using a recently developed $2 \times 2D$ dynamo model of the solar magnetic cycle. We find that even a single “rogue” bipolar magnetic region (BMR) in the simulations can have a major effect on the further development of solar activity cycles, boosting or suppressing the amplitude of subsequent cycles. In extreme cases an individual BMR can completely halt the dynamo, triggering a grand minimum. Rogue BMRs also have the potential to induce significant hemispheric asymmetries in the solar cycle. To study the effect of rogue BMRs in a more systematic manner, a series of dynamo simulations were conducted, in which a large test BMR was manually introduced in the model at various phases of cycles of different amplitudes. BMRs emerging in the rising phase of a cycle can modify the amplitude of the ongoing cycle while BMRs emerging in later phases will only impact subsequent cycles. In this model, the strongest impact on the subsequent cycle occurs when the rogue BMR emerges around cycle maximum at low latitudes but the BMR does not need to be strictly cross-equatorial. Active regions emerging as far as 20° from the equator can still have a significant impact. We demonstrate that the combined effect of the magnetic flux, tilt angle and polarity separation of the BMR on the dynamo is *via* their contribution to the dipole moment, δD_{BMR} . Our results indicate that prediction of the amplitude, starting epoch and duration of a cycle requires an accurate accounting of a broad range of active regions emerging in the previous cycle.

¹ Department of Astronomy, Institute for Geography and Earth Sciences, Eötvös University, Budapest, Hungary

² Département de Physique, Université de Montréal, Montréal, QC, Canada

³ Collège de Bois-de-Boulogne, Montréal, QC, Canada.

Keywords: Active Regions, Models; Solar Cycle, Models;

1. Introduction

The significantly lower amplitude of the ongoing Solar Cycle 24 in comparison to previous cycles has prompted increased interest in the origin of cycle-to-cycle variations in solar activity. Experience has shown that the best candidate for a physical precursor of the amplitude of an upcoming cycle is the peak strength of the solar polar magnetic fields (or alternatively, the solar dipole moment), reached typically around the time of solar minimum (Svalgaard, Cliver, and Kamide 2005; Petrovay 2010; Petrie, Petrovay, and Schatten 2014).

The critical issue still open is how, in turn, the amplitude of the dipole field is determined by solar activity in the previous cycle. In the currently most widely discussed flux transport dynamo scenario, the polar fields are built up by the poleward transport of f -polarity magnetic flux from active regions. This transport is mainly due to meridional circulation, so variations in meridional circulation have been invoked as a key factor in inter-cycle activity variations (Dikpati *et al.* 2010, Jiang *et al.* 2010, Hathaway and Upton 2014, Upton and Hathaway 2014).

An alternative possibility has been highlighted by Cameron *et al.* (2010) who stressed the importance of the tilt angle α of bipolar active regions relative to the east-west direction.¹ Clearly, for a $\alpha = 0$, f - and p -polarity flux would be transported towards the poles in equal rates, resulting in no net change in the polar flux. An increasing tilt angle will then lead to an increasing polar field strength. This opens two intriguing possibilities. On the one hand, tilt angles are known to be anticorrelated to cycle amplitude (Dasi-Espuig *et al.* 2010). The origin of this anticorrelation may be related to the dynamics of the emerging flux loop or to the meridional inflows towards the active latitude zone associated with the torsional oscillation pattern, the amplitude of which is determined by the level of solar activity. This “tilt quenching” is an important nonlinear feedback effect of solar activity level on the tilt angles, and thereby on the buildup of polar fields that will serve as seed fields for the next cycle.

On the other hand, a random scatter of tilt angles around the mean value determined by the above process will introduce some degree of stochasticity in the process. In particular, a few “rogue” active regions disobeying Joy’s law or Hale’s polarity rule (McClintock, Norton, and Li 2014, Jiang, Cameron, and Schüssler 2014) can potentially play havoc with the buildup of polar fields, especially if they emerge near the equator. The theoretical background of this, as outlined by Cameron and Schüssler (2015), is that the net solar dipole moment can only be affected by active regions emerging fully in one hemisphere if one of their polarities is preferentially cancelled between the two hemispheres by diffusion across the equator. This effect is stronger for ARs emerging near the equator.

¹Throughout this paper, α is taken to increase in the clockwise direction. For normally oriented active regions obeying Joy’s law, α is then positive on the N hemisphere and negative on the S hemisphere.

Furthermore, the odd AR emerging *across* the equator contribute directly to the solar dipole moment without invoking the necessity of cross-equatorial magnetic diffusion. In such cases, separation of the two polarities is aided by the poleward surface meridional flow. As the total magnetic flux in the polar cap is comparable to the magnetic flux in a single large active region (Wang and Sheeley 1991), even one AR emerging near (or, indeed, across) the equator can have a major distorting effect of polar flux buildup. The effect of rogue ARs at higher latitudes is, however, much less dramatic (Yeates, Baker, and van Driel-Gesztelyi 2015).

All this suggests a scenario where intercycle variations are normally governed by the nonlinear feedback effect on the tilt angles, offering a chance to forecast the amplitude of upcoming cycles in many cases, while once in a while rogue AR introduce large statistical fluctuations in the process, leading to unpredictable variations in the level of solar activity. One may speculate that in extreme cases such freak events may even trigger longer episodes of unusually low or unusually high activity, *i.e.* grand minima or grand maxima.

Pure mean-field dynamo models are inadequate for the study of such effects. Instead, individual active regions, manifest in the models as “bipolar magnetic regions” (BMRs) must be incorporated in the models in a way that correctly reproduces their statistical mean characteristics while allowing for stochastic variations. One such dynamo model, the “ $2\times 2D$ ” dynamo model has recently been developed by Lemerle, Charbonneau, and Carignan-Dugas (2015); Lemerle and Charbonneau (2017, hereafter L2015 and L2017, respectively). The purpose of the present paper is to study the effect of individual BMR, with special regard to rogue BMR on intercycle variations in the $2\times 2D$ dynamo model. An added advantage of this study is that it allows us to consider extremely long time series, covering hundreds of activity cycles. In contrast, the observational record of solar activity at our disposal with sufficient details regarding the sizes, positions and magnetic polarities of the spots only covers about half a dozen solar cycles, with less detailed data extending back to about 20 solar cycles.

The structure of the paper is as follows. Section 2 briefly recalls the main features of the $2\times 2D$ dynamo model used. In Section 3 we discuss salient features of the solutions with respect to stochasticity and cycle-to-cycle variations, highlighting the role of rogue BMRs. Section 4 discusses the most extreme effects of rogue BMR citing a few cases where such BMR naturally arise within the $2\times 2D$ dynamo model. In Section 5 a systematic series of numerical experiments are performed wherein a large “test” BMR departing strongly from Joy’s law is manually introduced in the simulation at various times, locations and with various other parameters, and the effects on the magnetic cycle are analyzed. Section 6 concludes the paper.

2. The Model Used

The Lemerle and Charbonneau (2017) solar cycle model couples a conventional surface flux transport (SFT) 2D simulation defined over a spherical surface (see L2015) to an equally conventional 2D axisymmetric Flux Transport Dynamo (FTD) simulation defined in a meridional plane (Charbonneau, St-Jean, and

Zacharias 2005). In the resulting hybrid kinematic $2 \times 2D$ Babcock-Leighton dynamo model, the SFT component provides the surface poloidal source term for the FTD simulation through the latter's surface boundary condition, while the FTD component provides the magnetic emergence events required as input to the SFT simulation.

It should be noted that other attempts at extending the mean field dynamo models to 3D with the inclusion of individual active regions do exist (Yeates and Muñoz-Jaramillo 2013, Miesch and Dikpati 2014). The main advantage of the $2 \times 2D$ model lies in its numerical efficiency and in the fact that it has been carefully calibrated to resemble the actual Sun. As the model includes a complete latitude-longitude representation of the simulated solar surface, the impact of varying characteristics of emerging BMRs (flux, pole separation, tilt angle, *etc.*) can be accounted for; as it does not solve the induction equation in three spatial dimensions, relatively high spatial resolution can be achieved within each model component, while allowing simulations extending over many thousands of simulated cycles. Detailed description of the model components can be found in the afore-cited papers (and especially L2015). In this section we merely provide an overview of the features that are most relevant to the investigations described further below.

The physical conditions driving the BMR emergences from the convective zone and their further temporal evolution in the solar photosphere are well described by the MHD induction equation:

$$\frac{\partial \mathbf{B}}{\partial t} = \nabla \times (\mathbf{u} \times \mathbf{B} - \eta \nabla \times \mathbf{B}). \quad (1)$$

The large-scale flow \mathbf{u} includes contributions from meridional circulation and differential rotation. The former is described by a modified form of the flow profile of van Ballegoijen and Choudhuri (1988), while for the latter we adopt the helioseismically-calibrated parametric form of Charbonneau *et al.* (1999). Both of these are considered axisymmetric and steady, as per the kinematic approximation. The total magnetic diffusivity η in the internal dynamo simulation follows the parametric profile $\eta(r)$ of Dikpati and Charbonneau (1999). In the SFT component we set $\eta_R \approx 10^{12} - 10^{13} \text{cm}^2 \text{s}^{-1}$, reflecting the strong effective diffusive transport provided by the supergranular flow.

The axisymmetric magnetic field simulated in the FTD component of the model is expressed as:

$$\mathbf{B}(r, \theta, t) = \nabla \times [A_\phi(r, \theta, t) \hat{\mathbf{e}}_\phi] + B_\phi(r, \theta, t) \hat{\mathbf{e}}_\phi, \quad (2)$$

where $\mathbf{B}_P = B_r \hat{\mathbf{e}}_r + B_\theta \hat{\mathbf{e}}_\theta$ and $B_\phi \hat{\mathbf{e}}_\phi$ are the poloidal and toroidal vector components of the field, respectively. Substitution into Equation 1 leads to two evolution equations for the scalar components $A_\phi(r, \theta, t)$ and $B_\phi(r, \theta, t)$:

$$\begin{aligned} \frac{\partial A_\phi}{\partial t} &= -\frac{1}{\varpi} (\mathbf{u}_P \cdot \nabla) (\varpi A_\phi) + \eta \left(\nabla^2 - \frac{1}{\varpi^2} \right) A_\phi, \\ \frac{\partial B_\phi}{\partial t} &= -\varpi (\mathbf{u}_P \cdot \nabla) \left(\frac{B_\phi}{\varpi} \right) + \eta \left(\nabla^2 - \frac{1}{\varpi^2} \right) B_\phi \end{aligned} \quad (3)$$

$$- (\nabla \cdot \mathbf{u}_P) B_\phi + \frac{1}{\varpi} \frac{\partial \eta}{\partial r} \frac{\partial (\varpi B_\phi)}{\partial r} + \varpi \mathbf{B}_P \cdot \nabla \Omega, \quad (4)$$

where $\varpi = r \sin \theta$, \mathbf{u}_P is the meridional flow and $\Omega(r, \theta)$ is the angular velocity. The magnetic field in the SFT code is considered radial, hence only the r -component of Equation 1 is solved at $r = R$:

$$\begin{aligned} \frac{\partial B_R}{\partial t} &= -\frac{1}{R \sin \theta} \frac{\partial}{\partial \theta} [u_\theta(R, \theta) B_R \sin \theta] - \Omega(R, \theta) \frac{\partial B_R}{\partial \phi} \\ &+ \frac{\eta_R}{R^2} \left[\frac{1}{\sin \theta} \frac{\partial}{\partial \theta} \left(\sin \theta \frac{\partial B_R}{\partial \theta} \right) + \frac{1}{\sin^2 \theta} \frac{\partial^2 B_R}{\partial \phi^2} \right] \\ &- \frac{B_R}{\tau_R} + S_{\text{BMR}}(\theta, \phi, t). \end{aligned} \quad (5)$$

The linear sink term $-B_R/\tau_R$ allows for exponential decay of the surface field (Baumann *et al.* 2004, Baumann, Schmitt, and Schüssler 2006), mimicking subduction of the polar cap magnetic field by the meridional flow. The other additional term $S_{\text{BMR}}(\theta, \phi, t) = \sum_i B_i(\theta, \phi) \delta(t - t_i)$ is the source of new BMR emergence events with δ the Dirac delta. The internal module receives the longitudinally averaged SFT solution $\langle B_R \rangle(\theta, t)$ at every FTD time step. This step provides the upper boundary condition. The coupling from the FTD towards the SFT simulation is the emergence of new BMRs. This is based on a semi-empirical emergence function $F_B(\theta, t)$ that gives the probability that the emergence of an active region will occur, given the internal distribution of magnetic fields within the FTD component of the model. Whenever one such emergence takes place, the characteristics of the emerging bipolar magnetic region —flux, pole separation, tilt angle— are randomly drawn from distribution functions for these quantities built from observed statistics of solar active regions (see Appendix A in L2015).

The emergence function incorporates a field strength threshold, below which the emergence probability falls rapidly to zero. This implies that the dynamo is not self-excited, in that it cannot amplify a seed magnetic field if the strength of the latter lies below this threshold. Along with this lower operating threshold, the only other nonlinearity introduced in the model is a reduction of the average active region tilt angle (α) with internal magnetic field strength:

$$\alpha_q = \frac{\alpha}{1 + (B_\phi/B_q)^2} \quad (6)$$

where B_q is the quenching field amplitude. Although this specific mathematical form is largely *ad hoc*, the idea of tilt quenching is supported by simulations of the rise and emergence of thin flux tubes. Physically, it reflects the fact that more strongly magnetized flux tubes rise more rapidly through the convection zone, and suffer less distortion by the Coriolis force during their rise (see Fan 2009, and references therein).

The reference solar cycle solution presented in L2017, which is adopted in the numerical experiments carried out in the present work, is defined by 11 adjustable parameters, which were optimized using a genetic algorithm designed

to minimize the differences between the spatiotemporal distribution of emergences produced by the model, and the observed sunspot butterfly diagram. Figure 1 presents a 40-yr long representative segment of this reference simulation. Panels (A) and (B) show time-latitude plots (butterfly diagrams) for the zonally-averaged surface magnetic field and for BMR emergence locations, respectively.

We note that emergence at low latitudes only results from the interplay between the internal magnetic field distribution within the FTD component and the emergence function. We do not impose a mask to restrict BMR emergences to low heliographic latitude, although our emergence function does include a high latitude cutoff at $\pm 70^\circ$ latitude, as suggested by stability analyses of thin flux tubes below the solar convection zone (see L2015 for further discussion).

It should also be noted that due care is warranted to ensure magnetic flux conservation within the SFT component of the model to a high level of numerical accuracy. This is because the polar cap flux, feeding back from the STF into the FTD model component, accounts for less than one percent of the total emerging (unsigned) BMR flux in the course of a typical cycle. Numerically accurate reproduction of the dipole moment to a relative accuracy of 10^{-3} (say) then requires numerical flux conservation at better than the 10^{-5} level (see L2017).

A pseudo-sunspot number time series can be constructed by simply summing the number of emergences taking place over subsequent one-day intervals in the simulation. Because we do not distinguish between individual spots and groups in the simulation, we simply rescale the amplitude of this time series to yield values commensurate with the international sunspot number. The resulting time series, smoothed with a 13-month running boxcar filter, is plotted as the black solid line in panel (C) of Figure 1 for the same simulation segment as on the upper two panels.

The axial dipole characterizing the SFT component is readily computed as:

$$D^*(t) = \frac{D(t)}{R^2} = \frac{3}{2} \int_0^\pi \langle B_R \rangle^\phi(\theta, t) \cos \theta \sin \theta d\theta, \quad (7)$$

that is also plotted in panel (D) of Figure 1. As shown in L2017 Section 4.2 and in agreement with the Sun, the magnitude of this dipole correlates very well (linear correlation coefficient $r \approx 0.9$) with the amplitude of the subsequent (pseudo-) SSN cycle amplitude, but not with the amplitude of the cycle during which the dipole is building up ($r \approx 0.25$). This indicates that the primary stochasticity driving cycle amplitude fluctuations operates in the course of the dipole buildup. This is readily seen on the bottom panel of Figure 1: the first two pseudo-SSN cycles have about the same amplitude of pseudo-sunspot numbers, but the dipole moments they generate in their descending phase differ by a factor of two. In contrast, the second and third pseudo-SSN cycles (solid black curve) differ by a factor of four in amplitude, yet generate dipoles peaking at almost exactly the same strength. This indicates that, in this simulation model (and most likely in the Sun as well as), it is not only the number of BMRs that sets the strength of the dipole moment, but rather the combination of physical parameters (polarity separation, tilt, *etc.*) of the emerging active regions. We now turn to a more detailed analysis of this behavior and its consequences for cycle predictability.

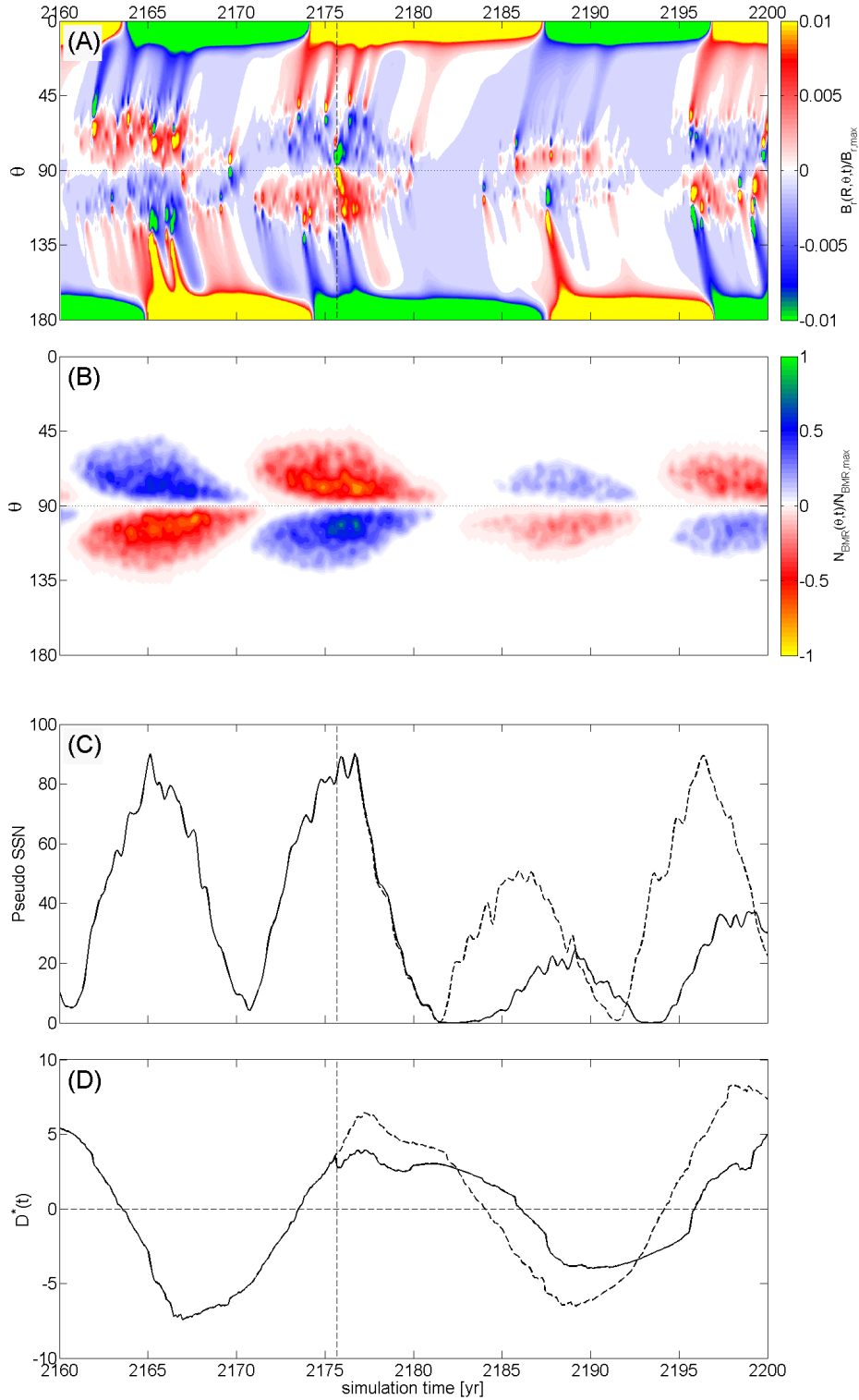


Figure 1. In panel (A) the surface time-latitude magnetogram is plotted for a representative segment of a reference simulation run. Panel (B) shows the butterfly diagram of BMR emergences, colored according to the trailing polarity, for the same period of time. The pseudo-SSN (C) and dipole moment (D) plotted with solid lines correspond to the data shown in panels (A) and (B). The dashed lines on panels (C) and (D) result from artificially removing a single large BMR emergence from the simulation (see Section 3).

3. Stochasticity and Predictability

The L2017 solar cycle model is a kinematic dynamo, in the sense that the large-scale flows introduced therein —differential rotation and meridional circulation— are assumed steady. This implies that the transport of the poloidal component from the surface to the deep interior as well as its shearing by internal differential rotation, and therefore the poloidal-to-toroidal part of the dynamo loop, are fully deterministic processes; any variation in the internal toroidal field so generated can only arise from a corresponding variation of the surface dipole. The production of the latter, on the other hand, is strongly influenced by the specificities of active region emergences: their magnetic flux, pole separation, tilt angle with respect to the E-W direction, *etc.* This represents a source of stochastic fluctuations, which in fact dominates the cycle-to-cycle variations produced by the model.

That this should be the case is not *a priori* obvious, and reflects a specificity of the global surface magnetic flux budget of the Sun. As pointed out by Wang, Nash, and Sheeley (1989), for a typical solar activity cycle the observed polar cap flux at the time of peak dipole strength is a few $\approx 10^{22}$ Mx; this is similar to the unsigned flux in one pole of a single large active region, and roughly one percent of the total unsigned flux emerging in active regions in the course of a typical solar activity cycle. Accurate modelling of the surface magnetic flux evolution thus requires that all properties of emerging active regions be known accurately if the buildup of the dipole in the descending phase is to be modeled (or predicted) with good accuracy.

This sensitivity can be readily illustrated by the following numerical experiment, the results of which are displayed on Figure 2. The black solid line is a time series segment of the smoothed monthly pseudo-sunspot number produced by a representative simulation run of the L2017 model. Now suppose that this reference run is the “real” sunspot number time series, and one is attempting to use the model to forecast future cycles by running ensembles of Monte Carlo simulations in which the characteristics of active regions are drawn randomly from empirically constructed distributions for the relevant quantities. The three semi-transparent colored bands are the min/max ranges in three such ensembles of five simulations in which, at a time indicated by the correspondingly colored vertical line segments, the random number generator controlling the draw of numerical values for magnetic fluxes, tilt angle, *etc.*, for the emerging active regions, is reset to another seed value. All model parameters remain the same, so that the diverging subsequent evolutions reflect only the different statistical realizations of the active region emergence process.

In all cases, a significant time delay between the reset and the divergence of the associated pseudo-SSN time series is observed. The extent of this time delay reaches a full cycle period when the reset takes place at minimum activity (green band), with the reset solutions tracking the original very well all the way to the subsequent minimum. If on the other hand the reset takes place at solar maximum (blue) or during the first half of the descending phase (red), divergence sets in already during the rising phase of the subsequent cycle, and the resulting range of cycle peak amplitudes ends up being a large fraction of

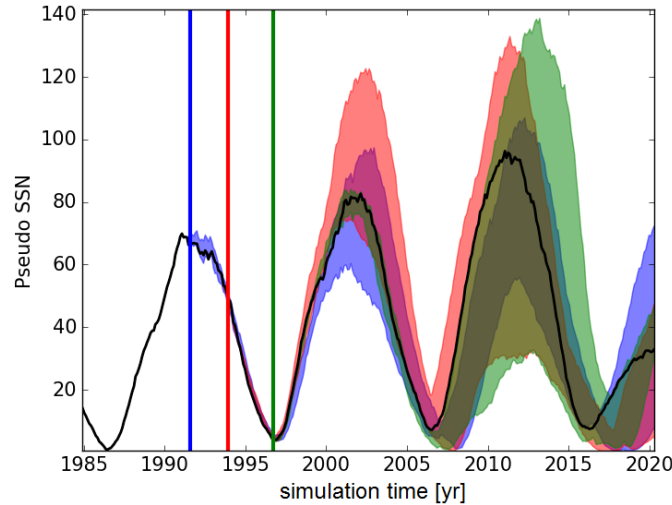


Figure 2. Divergence of the pseudo-SSN time series in the L2017 solar cycle model. The black curve is a reference time segment for a single run, and the colored bands give the min/max range for three ensembles of five solutions in which the random number generator controlling the statistics is reset at the time indicated by the correspondingly colored vertical line segments. In all cases divergence typically sets in approximately one pseudo-SSN cycle period after this reset.

the peak amplitude for the unperturbed reference solution (black solid line). The largest prediction window is thus possible working off cycle minimum, in which case the amplitude and duration of the subsequent cycle are well and reliably reproduced. Beyond the cycle following the reset of the emergence statistics (here from $t = 2006$ onward), all solutions diverge strongly, with even the timing of pseudo-SSN minima and maxima being affected even though the meridional flow speed remains the same in all cases.

Evidently, beyond about one cycle period the solutions diverge to the point of making any long-term prediction a futile undertaking, at least in the Monte Carlo form implemented here in which active region emergent properties are drawn randomly from empirically constructed statistical distributions. Nonetheless, in all these solutions, once the surface dipole is built at the end of a cycle’s descending phase, the evolution of the subsequent cycle—including peak amplitude, timing of maximum, duration, *etc.*—is set. This is the case in the Lemerle *et al.* model, unavoidably so in view of its aforementioned kinematic nature. It also seems to be the case in the Sun, as indicated by the fact that the cycle prediction methods based on measures of the solar surface dipole at times of activity minimum (*e.g.* Schatten *et al.* 1978; Svalgaard, Cliver, and Kamide 2005; Choudhuri, Chatterjee, and Jiang 2007), whatever their specific implementation may be, tend to fare better than most, and have done so again with the unusually low sunspot Cycle 24 (for a review see Petrovay 2010).

In this context, any hope of extending the predictability window beyond one cycle period clearly lies with an accurate prediction of the dipole moment build-

ing up in course of a cycle, and understanding which characteristics of emerging active regions have the most potential impact on this process. Put differently, we need to understand which active regions have the potential of completely derailing a prediction scheme based on assimilation of emerging active region data in the course of a cycle (Upton and Hathaway, 2014). The simulation segment plotted on Figure 1 offers an extreme —through not unreasonably so— specific example. Consider again the pseudo-SSN time series (black solid line in panel (C)), the corresponding time series for the surface dipole moment (panel (D)) and surface magnetogram (panel (A)) in Figure 1. Here the cycle peaking at year 2176 is followed by an extended minimum phase leading to a subsequent cycle of much reduced amplitude, qualitatively resembling the behavior observed with sunspot Cycles 23 and 24. In this specific simulation, at the time indicated by the vertical dashed line segment, near cycle maximum a very large ($\approx 10^{23}$ Mx, see Table 1, 2nd column) “rogue” active region emerged very close to the equator, and with the trailing polarity closer to the equator (anti-Joy tilt angle). This immediately leads to a significant drop in the dipole moment, which “stalls” what was up to then a typical buildup of the dipole. Moreover, the low amplitude, Solar Cycle-24 like cycle, beginning at $t \approx 2182$ is clearly also quite asymmetric as seen in the butterfly diagram, panel (B) of Figure 1. In our example, the new active regions appear first in the south, while in the north they appear a few years later only. This suggests that the emergence of the rogue BMR also affected the hemispheric asymmetry we observe during the next cycle —*cf.* Section 4 below.

Consider now the artificial removal of this active region; this leads to a subsequent evolution shown by the dashed lines, for the pseudo-SSN, panel (C) and the dipole moment, panel (D). The large drop in the dipole moment building up in the descending phase of the cycle clearly has a strong impact on the subsequent cycle: upon removal, the cycle begins its rising phase almost two years before it did in the reference solution, and reaches a peak amplitude more than twice higher and over two years sooner.

The 2.4×10^{23} Mx flux of the rogue BMR appearing —and being removed— in this simulation is indeed very high, but still not unreasonably so in the solar context (Tlatov and Pevtsov 2014; Muñoz-Jaramillo *et al.* 2015; Toriumi *et al.* 2017). During the descending phase of the ongoing Cycle 24 a gigantic BMR emerged in October 2014. This active region (AR2192) had a magnetic flux of about 1.6×10^{23} Mx and it topped out at a size of 2750 micro-hemisphere. This was the biggest since AR6368 in November 1990 which had a size of 3080 micro-hemisphere, but even this was still about half of the “Great Sunspot of 1947” which occupied about 6100 micro-hemisphere. Nonetheless, the cross-equatorial active regions reported by Cameron *et al.* (2014) had fluxes of $2\text{--}3 \times 10^{22}$ Mx but still had huge effect on the dipole moment according to their surface flux transport (SFT) simulations. The somewhat extreme example of Figure 1 is thus a perfect illustration of their argument for potentially critical impact of emergences occurring close to (or across) the solar equator, with the model providing the additional benefit of self-consistently tracking the impact of such emergences on the dynamo loop. Note also here how the ≈ 2 yr cycle onset delay erased by the removal of this rogue active region persists here through the last cycle plotted,

even though this is a kinematic model in which the average cycle period is set by the meridional flow speed, which is held fixed throughout this whole simulation.

From Figure 1 it is clearly seen that after the indicator line at $t \approx 2175.5$ the temporal evolution of the dipole moments splits immediately. The separation happens due to the removal of a peculiar or “rogue” active region identified in the reference case. By “rogue” we refer to its extreme physical properties such as high flux and angular separation. In addition, it is also characterized by a high tilt angle in the opposite orientation to what is expected from Joy’s law. The properties of this active region are listed in the second column of Table 1.

Table 1. Physical quantities of active regions discussed in the paper. Colatitudes θ_{lead} and θ_{trail} are the latitudinal positions of leading and trailing polarities; F is the flux of the trailing polarity ($F_{\text{trail}} = -F_{\text{lead}}$); α is the tilt angle and d is the angular separation of leading and trailing polarities. δD_{BMR} , the contribution of the BMR to the global dipole moment, is defined according to Equation 11. J/H indicates whether the active region is (anti-)Joy/(anti-)Hale. In the case of the last column a J/H (J/a-H) test-BMR increases (decreases) the dipole moment during the experiments detailed in Section 5.

θ_{lead}	84.8°	82.5°	95.6°	112°	89.5°
θ_{trail}	89.5°	86.3°	104.1°	118.6°	82.1°
F [10^{23} Mx]	2.43	-7.04	-3.58	4.39	-1.39
α	-8.65°	-10.92°	-15.53°	-11.08°	13.98°
d	31.64°	20.16°	32.11°	34.80°	30.97°
δD_{BMR} [10^{23} Mx]	-0.2014	0.4670	0.5293	-0.4633	-0.1810
J/H	a-J/H	a-J/H	J/H	J/H	J/H, J/a-H
	Figure 1	Figure 3	Figure 4	Figure 5	Section 5

4. Extreme Effects of Peculiar Active Region Emergences

In the case plotted in Figure 1 and discussed in the previous section, the rogue BMR had a significant effect on the further development of the activity cycles. This effect, however is still relatively moderate compared to some truly extreme cases to be presented in what follows.

4.1. Halt of Dynamo Action

In the case plotted in Figure 3 the dynamo is turned off by a BMR of extremely high flux and unfavorable tilt angle emerging after cycle maximum (see column 3 of Table 1). We denote the cycle phase of the emergence of the active region by ψ , the cycle phase being defined as the ratio of the time since the minimum and the duration of the cycle. This active region triggers an early polarity reversal which finally occurs during the same pseudo-sunspot cycle. After this event, the dipole moment does not build up again, instead decaying to zero during the following twenty years. The dashed black curve in Figure 3 shows that the dynamo keeps working if the identified peculiar BMR is removed from the simulation.

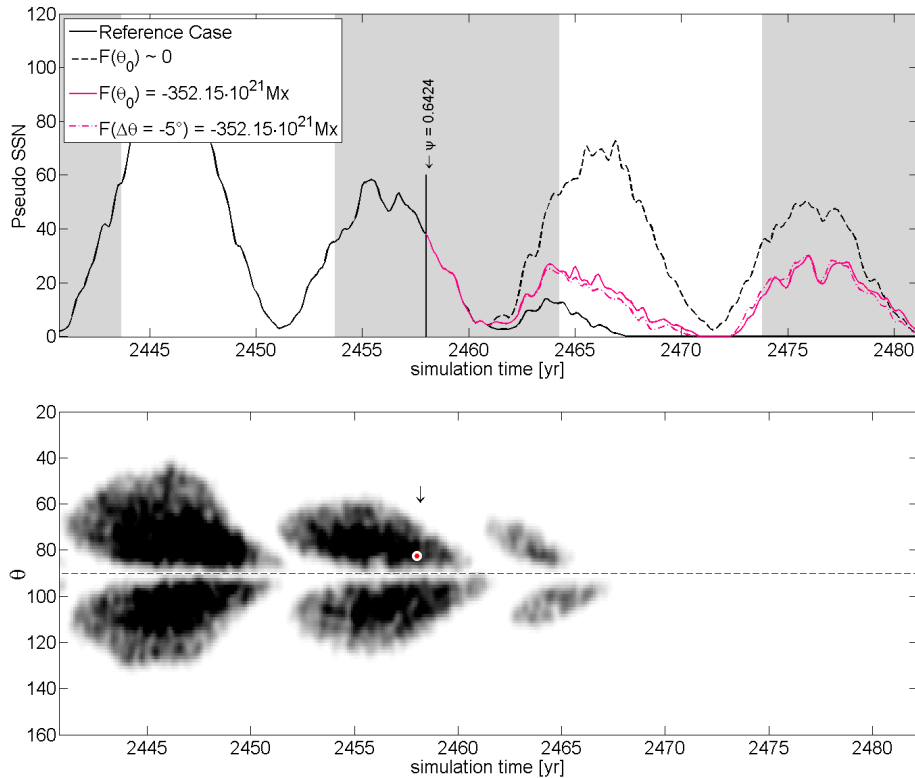


Figure 3. The spot that killed the dynamo: extreme effect of a huge active region during the descending phase of the cycle, on the SSN curve (top) and on the butterfly diagram (bottom). Red dot indicates the position of the leading polarity of the rogue BMR. The black dashed line in the top panel shows how the simulation unfolds if the rogue BMR is removed. The gray background corresponds to the negative dipole periods of this simulation as the dynamo in the reference case shuts down. The other curves indicate other simulations where the flux of the BMR was decreased (solid pink) and where this BMR with decreased flux emerged closer to the equator by 5° .

Two further experiments were done in this case in order to see whether or not a BMR with lower flux could cause the same effect at the same position, or closer to the equator. As it can be seen in Figure 3, an active region with a flux one half of the original BMR cannot produce the same effect, even if it is closer to the equator.

Such stopping events of the dynamo action were also found during the experiments detailed in Section 5. The dipole moment typically decayed after the test BMR emergence during the next 10-20 years, commensurate with the magnetic diffusion timescale for the bulk of the convection zone.

4.2. Restart of Dynamo Action

We identified another extreme case, when the dying dynamo is restarted by one peculiar BMR. In the reference case, indicated with solid black line at $t = 2176$ in

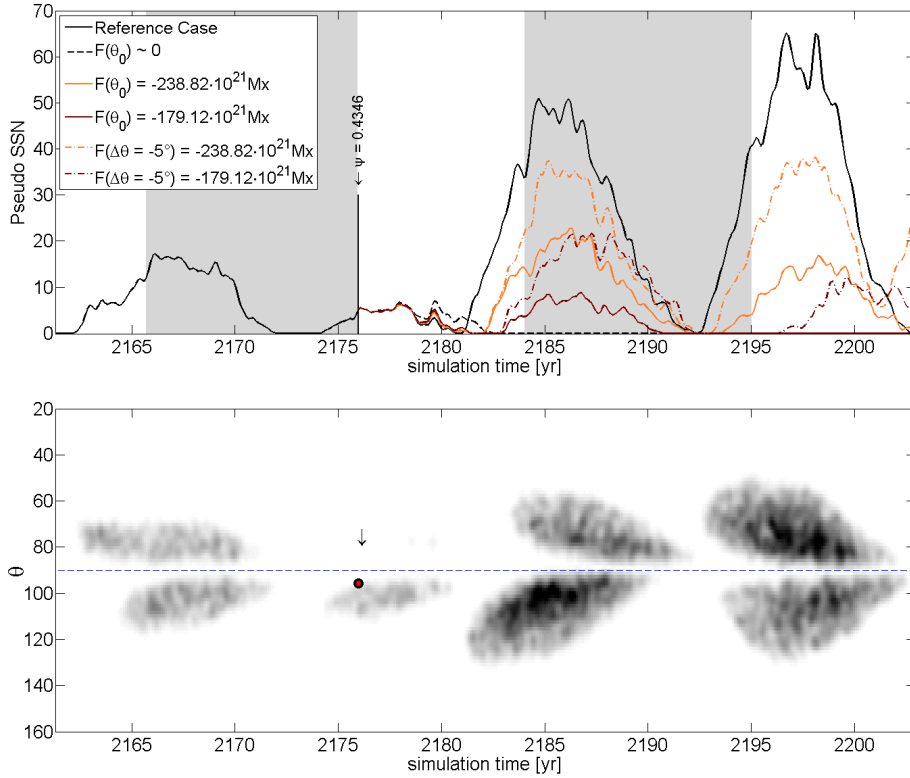


Figure 4. The spot that saved the dynamo: an example of the restart of an almost stopped dynamo simulation, due to large rogue BMR. Black dashed line shows the case when the active region was removed from the simulation. Solid curves of $F_{\text{trail}}(\theta_0)$ indicate cases when the flux of the rogue BMR was reduced, while $F_{\text{trail}}(\theta_0 - 5^\circ)$ with dash-dot lines show the cases when the BMR was closer to the equator by 5° . On the *bottom* the butterfly diagram of the reference case is shown. Red dot indicates the position of the leading polarity of the rogue BMR.

Figure 4, we found an active region of high flux and favorable tilt angle triggering an immediate polarity reversal and yielding a normal amplitude dipole moment after that (see column 4 of Table 1 for the characteristics of this BMR). Without this emergence the dipole moment would converge to zero in the next 20 years and no more active regions would emerge. This case is indicated by a dashed black line in Figure 4.

We run a few more simulations in the case of this active region in order to see whether or not a weaker BMR can produce the same result. We first divided the flux value by 1.5 and 2 at the same position (solid lines in Figure 4). At this position the BMR with the smallest flux can yield to one more pseudo-SSN cycle, and the dynamo action stops after this cycle. In the next step we inserted the decreased flux BMRs closer to the equator (dot-dashed lines in Figure 4). The emergences closer to the equator had a stronger effect, so that the weaker BMR could also restart the dynamo.

4.3. Effects on Hemispheric Asymmetry

The butterfly diagrams of Figures 1, 3 and 4 suggest that peculiar BMR emergences affect not only the amplitude or the starting epoch of the subsequent cycle, but the hemispheric asymmetry as well. In order to illustrate this effect, we chose the strongly asymmetric cycle plotted with the solid line in the top panel of Figure 5. Besides the asymmetry in the activity levels of the hemispheres we see in the third cycle, the new cycle starts about three years earlier on the south. This asymmetry was caused by a rogue BMR described in column 5 of Table 1. This active region emerged relatively far from the equator during the maximum of the second cycle, but still close enough to see significant effect. As the dashed line in the top panel of Figure 5 shows, by removing the identified strong BMR from the simulation, the northern hemisphere in the third cycle shows the same amount of active regions as before, but in the south one can see 30% lower amplitude compared to the reference case. According to Hathaway and Upton (2016), this asymmetry we see in this cycle might be predicted by the polar cap flux asymmetry during the perturbed cycle. As our plot shows in the bottom panel of Figure 5, the asymmetry in the reference case already appeared in the second cycle in the form of polar cap flux asymmetry. After the rogue BMR was removed, the polar cap flux asymmetry decreased in the course of the second cycle and consequently, the activity asymmetry was reduced in the third cycle as well.

To quantify this result we selected a series of 540 simulated cycles and compared the normalized asymmetry of the peak polar cap flux produced during the cycles (Δ_Φ) to two asymmetry parameters of the subsequent cycles. These parameters were the asymmetry of the total number of emergences at each hemisphere (Δ_{SSN}), and the time delay between the epochs when the new BMRs started to emerge on the North and the South (Δ_T).

The asymmetry of the polar cap flux at a given cycle is defined as follows:

$$\Delta_\Phi = \frac{|\Phi_{N,\max}| - |\Phi_{S,\max}|}{(|\Phi_{N,\max}| + |\Phi_{S,\max}|)/2}, \quad (8)$$

where $\Phi_{N,\max}$ ($\Phi_{S,\max}$) is the northern (Southern) polar cap flux maximum.

The asymmetry of the activity level:

$$\Delta_{SSN} = \frac{\Sigma SSN_N - \Sigma SSN_S}{(\Sigma SSN_N + \Sigma SSN_S)/2}, \quad (9)$$

where ΣSSN_N (ΣSSN_S) is the total number of emergences on the northern (southern) hemisphere.

The time lag between the hemispheres:

$$\Delta_T = \frac{t_N - t_S}{(T_N + T_S)/2}, \quad (10)$$

where t_N (t_S) is the beginning epoch of the cycle, while T_N (T_S) is the duration of the cycle on the North (South).

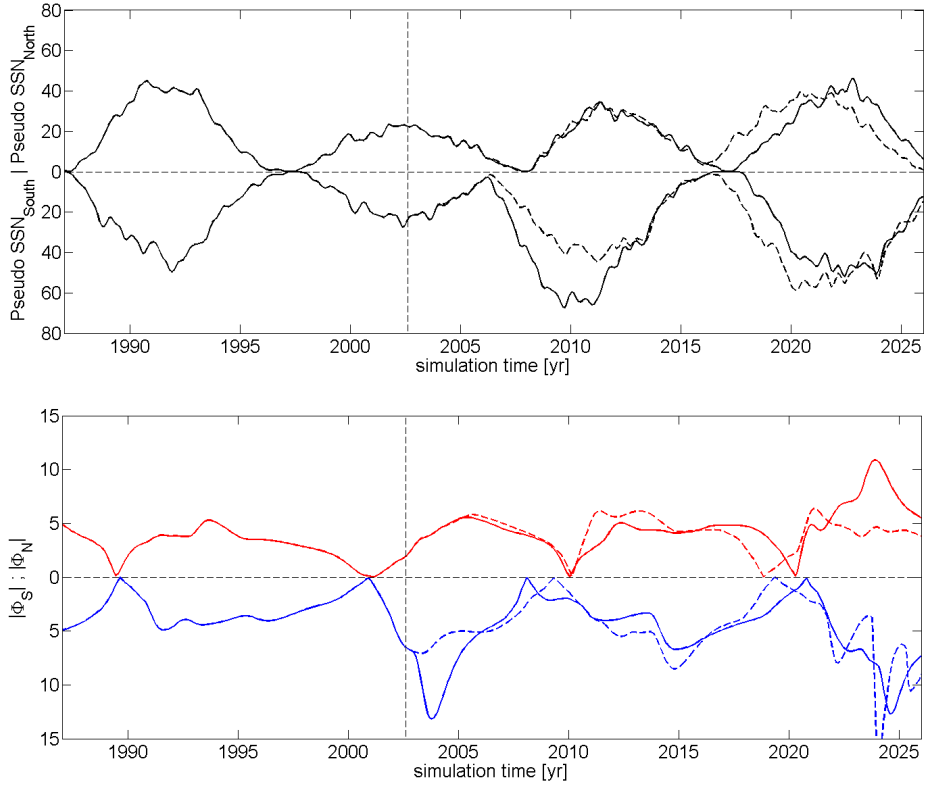


Figure 5. The *top* figure shows an example pseudo-SSN time series separately for the northern (+) and the southern hemispheres (–) to illustrate to what extent a strong BMR affects the asymmetry between the hemispheres. On the *bottom* the absolute values of the corresponding northern (+) (southern (–)) polar cap flux time series is shown. In both panels the solid lines show the reference case, while the dashed ones show the second run without the identified BMR. The polar cap flux is calculated as the surface integral of the magnetic field over a latitudinal extent of 20° from the poles.

Figure 6 shows the results in the form of two-dimensional count histograms. The correlation between the polar cap flux asymmetry during cycle i and the activity asymmetry during cycle $i + 1$ is $r = 0.7430$. In the case of the time lag obtained during cycle $i + 1$ is $r = -0.7174$. According to this result, the asymmetry level of the polar fields that build up during the cycles is a good predictor of the asymmetry for the subsequent cycle.

Hemispheric asymmetries were previously mostly discussed in the context of variations in the meridional flow (Belucz and Dikpati 2013, Hathaway and Upton 2016). The possibility that hemispheric asymmetries may be induced by rogue active regions offers an interesting and viable alternative, to be explored in more detail in future research.

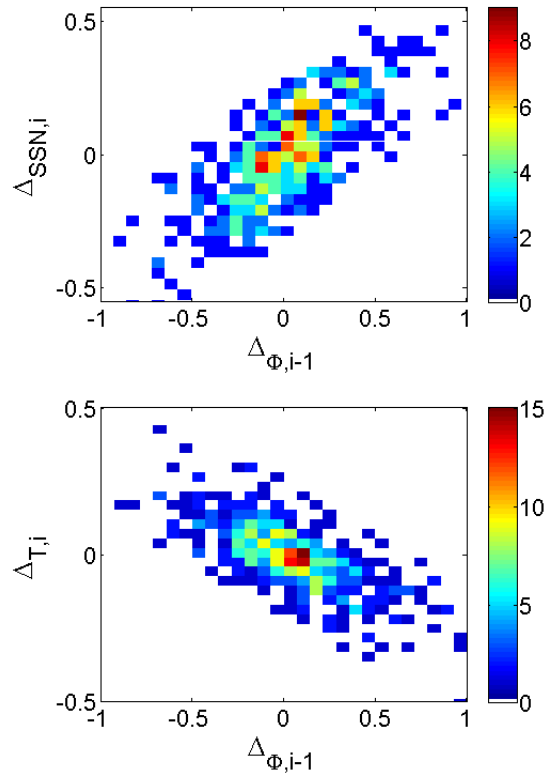


Figure 6. Two-dimensional histograms of the asymmetry of the hemispheric total pseudo-SSN (top) and the time lag between North and South (bottom) in pseudo-solar cycle i against the polar cap flux asymmetry during the previous cycle. Some outlier data have been removed. The number of cases (cycles) in each bin are indicated by the colour codes. The correlation coefficients are 0.7430 and -0.7174 , respectively.

5. Effects of a Rogue Active Region: a Systematic Analysis

In previous sections we discussed cases of rogue BMRs that spontaneously arose during the course of the simulation. In order to get a more systematic assesment of the effect of rogue BMR, in this section we will present results from a series of numerical experiments where an additional, “test” BMR was manually inserted into ongoing simulations with preset characteristics. The properties of this BMR are given in the sixth column of Table 1. (A BMR with such characteristics did actually emerge during the reference simulation at an earlier epoch.)

The investigation was performed for three cycles of average, below average and above average amplitudes, respectively. In each case two series of experiments were carried out with Hale (anti-Hale) test BMR in order to increase (decrease) the dipole moment of the examined cycle. As results were largely coherent among these series, in the accompanying plots only one of these cases (a test BMR which decreases the dipole moment of an average amplitude cycle) is shown.

In each series of experiments one parameter of the test BMR was systematically varied: emergence time, emergence latitude, magnetic flux, angular separation, or tilt angle.

5.1. Effects of Active Region Emergence Timing

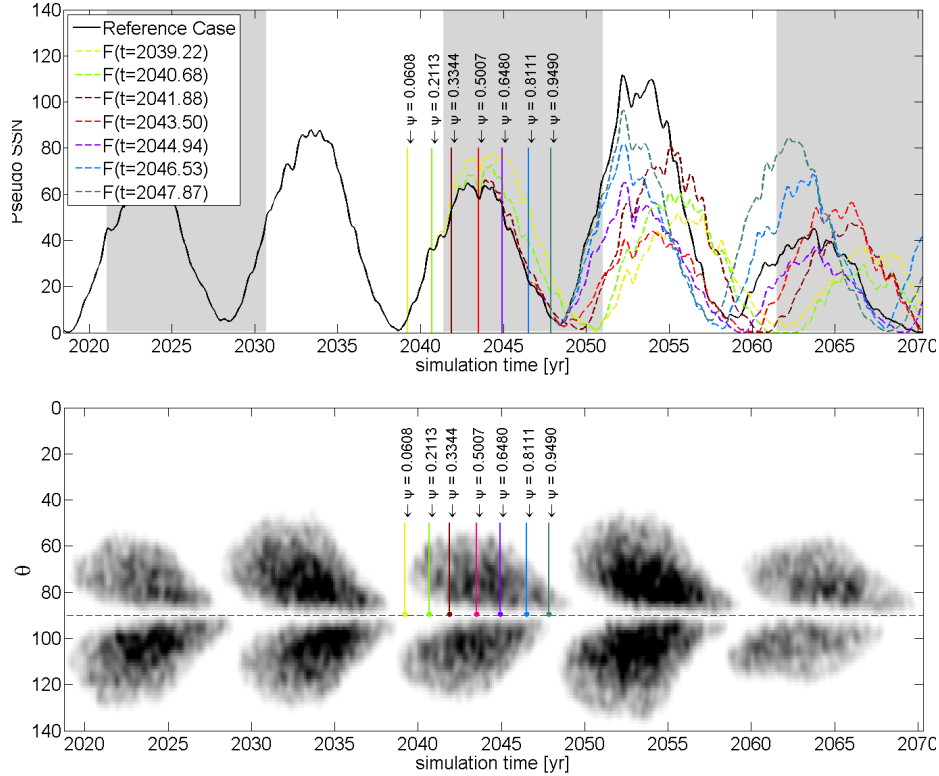


Figure 7. The *top* figure illustrates the effect of a single BMR inserted in the simulation at different phases of the cycle. The black solid line represents the reference case without the test BMR, gray background indicates the negative phase of the dipole moment. On the *bottom* the butterfly diagram of the reference case is shown. The dots indicate the position of the leading polarity of the active region. The properties of the active region are listed in column 6 of Table 1.

During the first experimental series the emergence time of the test BMR was varied. The emergence epochs were chosen based on the phase of the cycle ψ . In the example case shown in Figure 7, the inserted BMR decreases the dipole moment during the course of an average magnitude cycle.

If a peculiar BMR emerges during the rising phase of the simulated cycle it affects the amplitude of the ongoing cycle as well. The explanation to this is that peculiar BMRs occurring before dipole-moment polarity-reversal can modify its timing. Obviously, after the time of maximum the impact of such BMRs on the current cycle disappears. Since during the rising phase these active regions

affect the ongoing cycle itself, their probable effect on the subsequent one will be unpredictable.

If the emergence happens during the descending phase, it tends to have less impact on the subsequent cycle. It is clear from Figure 7 that the later the BMR emerges, the smaller the amplitude change expected during the next cycle. The strongest effect is expected if the perturbation occurs at cycle maximum. The amplitude of the next cycle can be lower (higher) by up to 100% when the emergence decreases (increases) the amplitude of the dipole moment being built up.

The length of the current cycle can also be modified but the impact decreases during the rising phase and after the pseudo-SSN maximum it disappears entirely. The ongoing cycle can be lengthened (shortened) by up to two years if the emerged peculiar BMR decreases (increases) the amplitude of the dipole moment. Due to this duration change, the beginning of the subsequent cycle also shifts by up to two years. This result is particularly interesting, since in this dynamo model the meridional flow speed is constant, and sets the cycle length in a simulation in which stochasticity in properties of BMRs is turned off. In general, not only the magnitude of the dipole moment changes, but also the timing of polarity reversals.

Emergences of peculiar BMRs before and after the maxima also result in different timings of the subsequent simulated cycle maximum due to the the shifting of the minimum epochs.

5.2. Effects of Active Region Flux

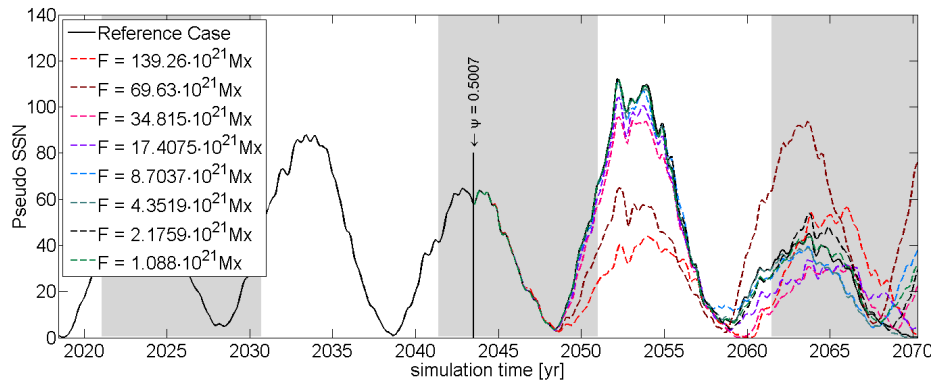


Figure 8. The figure shows how the impact of a single inserted BMR at cycle maximum changes depending on its flux. The red curve, corresponding to the lowest amplitude during the subsequent cycle, is identical to the $\psi = 0.5007$ case on Figure 7. Gray background indicates the negative phase of the dipole moment. The properties of the active region are listed in column 6 of Table 1.

The second set of simulation runs focuses on the role of the magnetic flux of the emerging active region. Here, the flux of the test BMR is decreased in logarithmic increments (a factor of two between adjacent cases), while other parameters are kept constant. The test BMR is inserted at cycle maximum

where the highest impact is expected. Figure 8 shows that the effect on the amplitude of the subsequent cycle decreases with decreasing magnetic flux of the test BMR.

On the other hand, this modification of the flux does not cause significant changes to the minimum epoch. As suggested in Figure 8 above, the subsequent cycle tends to start producing new active regions earlier (later) due to the effect of inserted active regions increasing (decreasing) the dipole moment. Identically, the duration of the minimum tends to be shorter (longer), when the test BMR increased (decreased) the dipole moment. The minimum duration is defined by the period when the pseudo-SSN is below 12.5. This is twice the lowest activity seen at $t = 2058.5$.

5.3. Effects of Tilt and Angular Separation

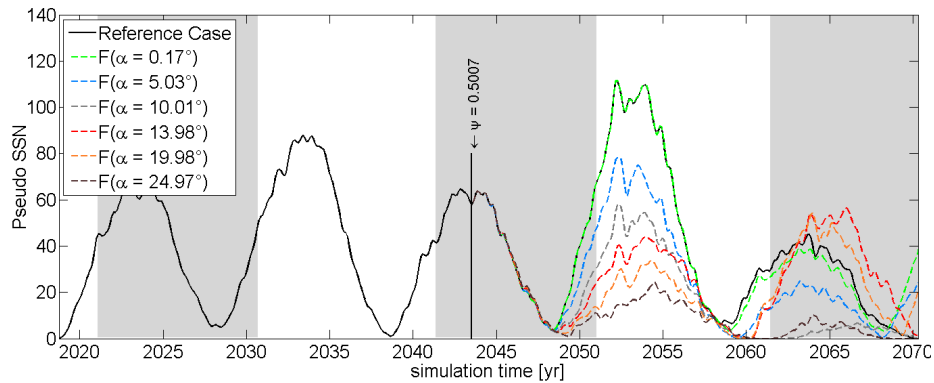


Figure 9. The plot shows how the tilt angle of the inserted BMR at cycle maximum affects the amplitude of the next cycle. The red curve is identical to the $\psi = 0.5007$ case on Figure 7. Gray background indicates the negative phase of the dipole moment. The properties of the active region are listed in column 6 of Table 1.

The importance of the latitudinal size, *i.e.* the tilt angle and the separation of the inserted active region polarities were also examined. As an example we plot a result from perturbing the tilt angle in Figure 9. As the tilt angle of the active region was increased from 0° to 25° in $\Delta\alpha = 5^\circ$ steps, the amplitude of the subsequent cycle changed to a higher extent relative to the reference case. Evidently, for $\alpha = 0^\circ$ the amplitude change of the next cycle is zero as the net contribution to the dipole moment is zero. For the case of the emerging test BMR with angular separation and flux parameters listed in column 6 of Table 1, at $\alpha = 25^\circ$ the amplitude of the subsequent simulated cycle can increase by up to 200% in cases when the emerged BMR increased the dipole moment. When the emergence decreases the dipole moment the dynamo action tends to stop in the case of weak following cycles.

The separation of the active region was changed in steps of $\Delta d = 5^\circ$ from $\approx 16^\circ$ to $\approx 41^\circ$. This kind of perturbation yields the same result as changing the tilt angle, since in both cases the latitudinal size of the active region changes,

which contributes to the efficiency of the polarity separation by the meridional circulation.

Similarly to the case of flux perturbation, active regions of the next cycle tend to emerge earlier (later) when the test region increased (decreased) the dipole moment. This effect, however, is more prominent if the perturbed property is the tilt angle, as Figure 9 shows.

5.4. Effects of Changes in Latitude

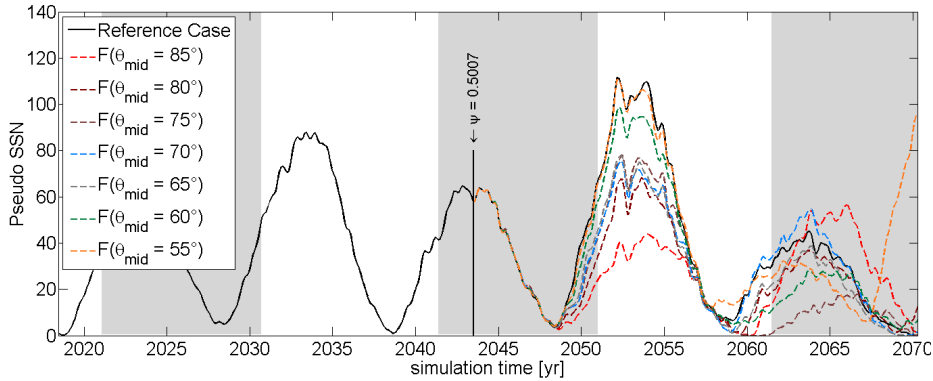


Figure 10. The figure shows how the latitude of the inserted BMR at cycle maximum affects the amplitude of the subsequent cycle. The red curve, corresponding to the lowest amplitude during the subsequent cycle, is identical to the $\psi = 0.5007$ case on Figure 7. Gray background indicates the negative phase of the dipole moment. The properties of the active region are listed in column 6 of Table 1.

According to Cameron *et al.* (2014) active regions very close to the equator have significant effect on the dipole moment. To verify this for our model we investigated the impact of decreasing the colatitude of the leading and trailing polarities in steps of $|\Delta\theta| = 5^\circ$ from $\theta_{\text{mid}} = 85^\circ$ to $\theta_{\text{mid}} = 55^\circ$. We found that 20° from the equator there is still about a 50% effect on the amplitude of the subsequent cycle. Note that although the angular separation stays the same by definition, the linear distance will decrease by 17% from the original to the highest position. The error caused by the decreased physical size is only 5% at $\theta_{\text{mid}} = 70^\circ$, *i.e.* 20° from the equator, where the effect on the next cycle is still significant.

In terms of changes in the length of the next cycle no systematic effect was found.

5.5. Discussion

Substituting an individual BMR into Equation 7, one finds that, to leading order, the contribution of this source to the global dipole moment scales as

$$\delta D_{\text{BMR}} \approx F d \sin \alpha \sin \theta, \quad (11)$$

where, as before, d is the angular separation of leading and trailing polarities, α is the tilt angle, θ is the co-latitude of the active region midpoint, and $F = F_{\text{trail}}$ is the flux of the trailing polarity ($F_{\text{trail}} = -F_{\text{lead}}$).

This suggests that the effects of the individual factors in Equation 11 can be combined in δD_{BMR} . This is indeed borne out in Figure 11. The top abscissa of both panels shows the middle colatitude of the test BMR inserted during the simulations discussed in Section 5.4. The bottom abscissa shows the contribution of the test active region to the global dipole moment (δD_{BMR}) converted by Equation 11 from the flux, tilt angle and separation changes described in Sections 5.2 and 5.3. In each case the constant parameters were taken from the sixth column of Table 1. The ordinates in Figure 11 show the relative change in amplitude of the next cycle (top panel) and the duration of the minimum (bottom panel) changes averaged for the simulation runs. The new cycle properties after inserting the test BMR, X_{test} (*e.g.* amplitude) are always compared to the

reference case, X_{ref} as follows: $\text{rms}_{\Delta} = \sqrt{\left\langle \left(\frac{X_{\text{ref}} - X_{\text{test}}}{X_{\text{ref}}} \right)^2 \right\rangle}$.

The good agreement of the green, magenta and blue curves of Figure 11 confirms that the contribution number δD_{BMR} is indeed an appropriate combined measure of the ‘‘dynamo efficiency’’ of individual active regions. On the observational front, the importance of the combined influence of F and α on the buildup of the poloidal field was demonstrated by Muñoz-Jaramillo *et al.* (2013) based on mean-tilt-weighted active region areas and polar facular counts as a proxy of the dipole moment for Cycles 15–23.

The red dotted curve showing the effect of emergence latitude clearly indicates that the impact on the peak value of the subsequent cycle decreases if the emergence occurs farther away from the equator. Nevertheless, in the model analyzed here BMR emerging around 20° latitude can still have significant effect on the subsequent cycle.

In this context it should be emphasized that Equation 11 only yields the *initial* contribution of the BMR to the dipole moment. As time proceeds, this contribution is significantly modified by diffusion and advection on the solar surface, until an asymptotic value is reached. This process was studied by Jiang, Cameron, and Schüssler (2014) in a surface flux transport model. They find (their Figure 6) that the final contribution to the global dipole decreases quite fast with increasing emergence latitude, becoming negligible at $15\text{--}20^\circ$. (See also Jiang *et al.* 2014.) These findings are in qualitative agreement with our results, although some quantitative differences, probably related to model details, remain to be clarified.

On the other hand, Hazra, Choudhuri, and Miesch (2017) report the opposite trend, based on a small set of numerical experiments similar to those described herein. While the origin of this discrepancy remains unclear at this juncture, it is worth pointing out that in their observational analysis Yeates, Baker, and van Driel-Gesztelyi (2015) find that high latitude BMRs do not have a long-term contribution to the polar field, lending support to the tendency reported in this paper and in Jiang, Cameron, and Schüssler (2014).

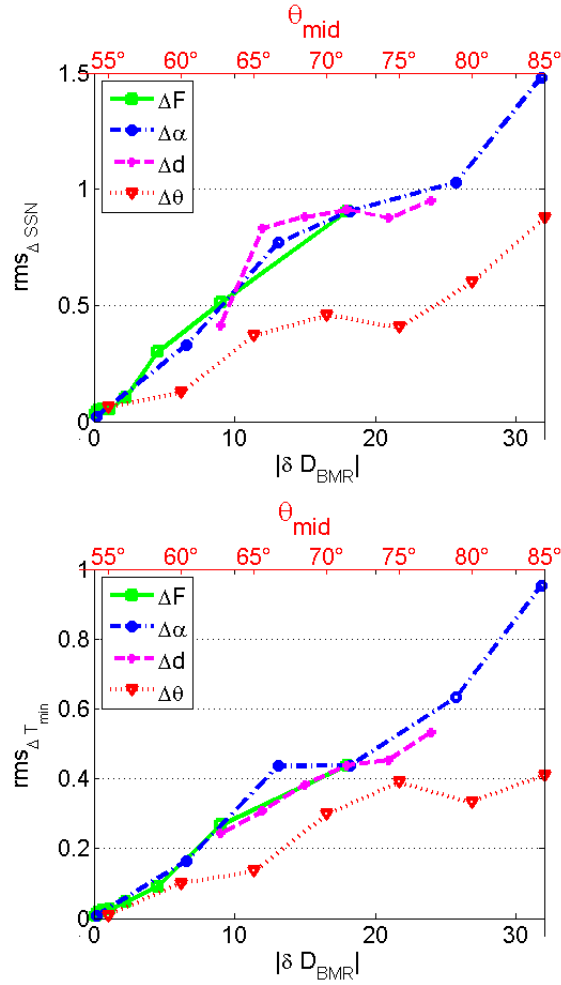


Figure 11. Average effect of BMR emergences on the amplitude of the subsequent cycle (top panel) and on the duration of the minimum (bottom panel). The flux change (green curve), the tilt angle variation (blue curve) and the separation modification (magenta curve) of the active region are converted to the contribution to the build up of the dipole moment according to Equation 11. The top axis, corresponding to the red dotted curve, indicates the colatitude of the BMR.

6. Conclusion

Using a new “2×2D” dynamo model of the solar activity cycle we studied the effect of rogue BMRs (large BMRs with unusual characteristics) on subsequent simulated solar cycles. We found that even a single rogue BMR can have a major effect on the further development of solar activity cycles, boosting or suppressing the amplitude of subsequent cycles. In extreme cases an individual BMR can completely halt the dynamo, triggering a grand minimum. Alternatively a dynamo on the verge of being halted can also be resuscitated by a rogue BMR

with favourable characteristics. Rogue BMRs also have the potential to induce significant hemispheric asymmetries in the solar cycle.

To study the effect of rogue BMRs in a more systematic manner, we have conducted a series of dynamo simulations where a large test BMR is manually introduced in the model at various phases of cycles of different amplitudes. A BMR emerging in the rising phase of a cycle can modify the amplitude of the ongoing cycle while a BMR emerging in later phases only impact subsequent cycles. The strongest impact on the subsequent cycle is found when the rogue BMR emerges around cycle maximum at low latitudes but the BMR does not need to be strictly cross-equatorial. Active regions emerging as far as 20° from the equator still have a significant effect on the subsequent cycle. We have demonstrated that the combined effect of the magnetic flux, tilt angle and polarity separation of the BMR on the dynamo is via the contribution to the dipole moment, δD_{BMR} . An increase in either of these quantities will lead to an enhancement of the effect on solar activity in the subsequent cycle. The sense of the effect, in turn, depends on the sign of the contribution to the dipole moment being built up in the late phases of the cycle.

The selected cases discussed in Sections 3 and 4 are in agreement with the general rules derived in Section 5. For instance, in panel (C) of Figure 1, at the maximum of the second cycle in the reference simulation the identified active region had a decreasing effect on the dipole moment, hence the magnitude of the subsequent pseudo-SSN cycle also decreased. In the second run, indicated by dashed black line, the identified BMR was removed from the simulation. As a consequence, the third cycle doubled in amplitude compared to the reference case. Besides this, the duration of the minimum decreased significantly, as well. In terms of hemispheric asymmetry, as it is shown in panel (B) for the reference case, the BMR emerging on the north decreased the northern polar cap flux delaying the onset of the subsequent pseudo-SSN cycle in the northern hemisphere.

It should be emphasized that while the rogue BMRs identified here are large, they do not exceed in size the largest solar active regions on record. Furthermore, as our detailed record only goes back to about a score of solar cycles, the largest ever observed active regions by no means represent a theoretical upper limit. Therefore, our results suggest that large active regions with peculiar characteristics may be responsible for unexpected changes in the behaviour of the solar dynamo, as already suggested by Jiang, Cameron, and Schüssler (2015). More detailed comparisons between simulated and observed solar cycles may be the subject of future research.

Acknowledgments This project was partially funded by the European Union’s Horizon 2020 research and innovation programme under grant agreement No. 739500, by the Discovery Grant Program of the Natural Sciences and Engineering Research Council of Canada, and by the Campus Mundi Program.

Conflict of interest The authors declare that they have no conflicts of interest.

References

Baumann, I., Schmitt, D., Schüssler, M.: 2006, A necessary extension of the surface flux transport model. *Astron. Astrophys.* **446**, 307. DOI.

- Baumann, I., Schmitt, D., Schüssler, M., Solanki, S.K.: 2004, Evolution of the large-scale magnetic field on the solar surface: A parameter study. *Astron. Astrophys.* **426**, 1075. DOI.
- Belucz, B., Dikpati, M.: 2013, Role of Asymmetric Meridional Circulation in Producing North-South Asymmetry in a Solar Cycle Dynamo Model. *Astrophys. J.* **779**, 4. DOI. ADS.
- Cameron, R., Schüssler, M.: 2015, The crucial role of surface magnetic fields for the solar dynamo. *Science* **347**, 1333. DOI.
- Cameron, R.H., Jiang, J., Schmitt, D., Schüssler, M.: 2010, Surface Flux Transport Modeling for Solar Cycles 15-21: Effects of Cycle-Dependent Tilt Angles of Sunspot Groups. *Astrophys. J.* **719**, 264. DOI.
- Cameron, R.H., Jiang, J., Schüssler, M., Gizon, L.: 2014, Physical causes of solar cycle amplitude variability. *J. Geophys. Res.(Space Physics)* **119**, 680. DOI.
- Charbonneau, P., St-Jean, C., Zacharias, P.: 2005, Fluctuations in Babcock-Leighton Dynamoes. I. Period Doubling and Transition to Chaos. *Astrophys. J.* **619**, 613. DOI.
- Charbonneau, P., Christensen-Dalsgaard, J., Henning, R., Larsen, R.M., Schou, J., Thompson, M.J., Tomczyk, S.: 1999, Helioseismic Constraints on the Structure of the Solar Tachocline. *Astrophys. J.* **527**, 445. DOI.
- Choudhuri, A.R., Chatterjee, P., Jiang, J.: 2007, Predicting Solar Cycle 24 With a Solar Dynamo Model. *Phys. Rev. Lett.* **98**, 131103. DOI.
- Dasi-Espuig, M., Solanki, S.K., Krivova, N.A., Cameron, R., Peñuela, T.: 2010, Sunspot group tilt angles and the strength of the solar cycle. *Astron. Astrophys.* **518**. DOI.
- Dikpati, M., Charbonneau, P.: 1999, A Babcock-Leighton Flux Transport Dynamo with Solar-like Differential Rotation. *Astrophys. J.* **518**, 508. DOI.
- Dikpati, M., Gilman, P.A., de Toma, G., Ulrich, R.K.: 2010, Impact of changes in the Sun's conveyor-belt on recent solar cycles. *Geophys. Res. Lett.* **37**, L14107. DOI. ADS.
- Fan, Y.: 2009, Magnetic Fields in the Solar Convection Zone. *Living Rev. Sol. Phys.* **6**. DOI.
- Hathaway, D.H., Upton, L.: 2014, The solar meridional circulation and sunspot cycle variability. *Journal of Geophysical Research (Space Physics)* **119**, 3316. DOI. ADS.
- Hathaway, D.H., Upton, L.A.: 2016, Predicting the amplitude and hemispheric asymmetry of solar cycle 25 with surface flux transport. *Journal of Geophysical Research (Space Physics)* **121**, 10. DOI. ADS.
- Hazra, G., Choudhuri, A.R., Miesch, M.S.: 2017, A Theoretical Study of the Build-up of the Sun's Polar Magnetic Field by using a 3D Kinematic Dynamo Model. *Astrophys. J.* **835**, 39. DOI.
- Jiang, J., Cameron, R.H., Schüssler, M.: 2014, Effects of the Scatter in Sunspot Group Tilt Angles on the Large-scale Magnetic Field at the Solar Surface. *Astrophys. J.* **791**, 5. DOI.
- Jiang, J., Cameron, R.H., Schüssler, M.: 2015, The Cause of the Weak Solar Cycle 24. *Astrophys. J. Lett.* **808**, L28. DOI. ADS.
- Jiang, J., İşik, E., Cameron, R.H., Schmitt, D., Schüssler, M.: 2010, The Effect of Activity-related Meridional Flow Modulation on the Strength of the Solar Polar Magnetic Field. *Astrophys. J.* **717**, 597. DOI.
- Jiang, J., Hathaway, D.H., Cameron, R.H., Solanki, S.K., Gizon, L., Upton, L.: 2014, Magnetic Flux Transport at the Solar Surface. *Space Sci. Rev.* **186**, 491. DOI.
- Lemerle, A., Charbonneau, P.: 2017, A Coupled 2×2D Babcock-Leighton Solar Dynamo Model. II. Reference Dynamo Solutions. *Astrophys. J.* **834**, 133. DOI.
- Lemerle, A., Charbonneau, P., Carignan-Dugas, A.: 2015, A Coupled 2×2D Babcock-Leighton Solar Dynamo Model. I. Surface Magnetic Flux Evolution. *Astrophys. J.* **810**, 78. DOI.
- McClintock, B.H., Norton, A.A., Li, J.: 2014, Re-examining Sunspot Tilt Angle to Include Anti-Hale Statistics. *Astrophys. J.* **797**, 130. DOI.
- Miesch, M.S., Dikpati, M.: 2014, A Three-dimensional Babcock-Leighton Solar Dynamo Model. *Astrophys. J. Lett.* **785**, L8. DOI. ADS.
- Muñoz-Jaramillo, A., Dasi-Espuig, M., Balmaceda, L.A., DeLuca, E.E.: 2013, Solar Cycle Propagation, Memory, and Prediction: Insights from a Century of Magnetic Proxies. *Astrophys. J. Lett.* **767**, L25. DOI.
- Muñoz-Jaramillo, A., Senkpeil, R.R., Windmueller, J.C., Amouzou, E.C., Longcope, D.W., Tlatov, A.G., Nagovitsyn, Y.A., Pevtsov, A.A., Chapman, G.A., Cookson, A.M., Yeates, A.R., Watson, F.T., Balmaceda, L.A., DeLuca, E.E., Martens, P.C.H.: 2015, Small-scale and Global Dynamoes and the Area and Flux Distributions of Active Regions, Sunspot Groups, and Sunspots: A Multi-database Study. *Astrophys. J.* **800**, 48. DOI.
- Petrie, G.J.D., Petrovay, K., Schatten, K.: 2014, Solar Polar Fields and the 22-Year Activity Cycle: Observations and Models. *Space Sci. Rev.* **186**, 325. DOI.

- Petrovay, K.: 2010, Solar Cycle Prediction. *Living Rev. Sol. Phys.* **7**, 6. DOI.
- Schatten, K.H., Scherrer, P.H., Svalgaard, L., Wilcox, J.M.: 1978, Using dynamo theory to predict the sunspot number during solar cycle 21. *Geophys. Res. Lett.* **5**, 411. DOI.
- Svalgaard, L., Cliver, E.W., Kamide, Y.: 2005, Sunspot cycle 24: Smallest cycle in 100 years? *Geophys. Res. Lett.* **32**, L01104. DOI.
- Tlatov, A.G., Pevtsov, A.A.: 2014, Bimodal Distribution of Magnetic Fields and Areas of Sunspots. *Solar Phys.* **289**, 1143. DOI.
- Toriumi, S., Schrijver, C.J., Harra, L.K., Hudson, H., Nagashima, K.: 2017, Magnetic Properties of Solar Active Regions That Govern Large Solar Flares and Eruptions. *Astrophys. J.* **834**, 56. DOI.
- Upton, L., Hathaway, D.H.: 2014, Effects of Meridional Flow Variations on Solar Cycles 23 and 24. *Astrophys. J.* **792**, 142. DOI. ADS.
- van Ballegoijen, A.A., Choudhuri, A.R.: 1988, The possible role of meridional flows in suppressing magnetic buoyancy. *Astrophys. J.* **333**, 965. DOI.
- Wang, Y.-M., Sheeley, N.R. Jr.: 1991, Magnetic flux transport and the sun’s dipole moment - New twists to the Babcock-Leighton model. *Astrophys. J.* **375**, 761. DOI.
- Wang, Y.-M., Nash, A.G., Sheeley, N.R. Jr.: 1989, Magnetic flux transport on the sun. *Science* **245**, 712. DOI.
- Yeates, A.R., Muñoz-Jaramillo, A.: 2013, Kinematic active region formation in a three-dimensional solar dynamo model. *Mon. Not. Roy. Astr. Soc.* **436**, 3366. DOI. ADS.
- Yeates, A.R., Baker, D., van Driel-Gesztelyi, L.: 2015, Source of a Prominent Poleward Surge During Solar Cycle 24. *Solar Phys.* **290**, 3189. DOI.